Title

Real-time augmented reality for delineation of surgical margins during neurosurgery using autofluorescence lifetime contrast

Permalink

https://escholarship.org/uc/item/6x75z0ft

Journal

Journal of Biophotonics, 13(1)

ISSN

1864-063X

Authors

Alfonso-Garcia, Alba
Bec, Julien
Weaver, Shamira Sridharan
et al.

Publication Date

2020

DOI

10.1002/jbio.201900108

Peer reviewed

Real-time augmented reality for delineation of surgical margins during neurosurgery using autofluorescence lifetime contrast

Alba Alfonso-Garcia[1], **Julien Bec**[1], **Shamira Sridharan**[1], **Brad Hartl**[1], **Jakob Unger**[1], **Matthew Bobinski**[2], **Mirna Lechpammer**[3], **Fady Girgis**[4], **James Boggan**[4], **Laura Marcu**[*,1,4]

[1]Dept. Biomedical Engineering, University of California, Davis, California, United States

[2]Dept. Radiology, University of California, Davis, California, United States

[3]Dept. Pathology and Laboratory Medicine, University of California, Davis, United States

[4]Dept. Neurological Surgery, University of California, Davis, California, United States

Abstract

Current clinical brain imaging techniques used for surgical planning of tumor resection lack intraoperative and real-time feedback; hence surgeons ultimately rely on subjective evaluation to identify tumor areas and margins. We report a fluorescence lifetime imaging (FLIm) instrument (excitation: 355 nm; emission spectral bands: 390/40 nm, 470/28 nm, 542/50 nm, and 629/53 nm) that integrates with surgical microscopes to provide real-time intraoperative augmentation of the surgical field of view with fluorescent derived parameters encoding diagnostic information. We show the functionality and safety features of this instrument during neurosurgical procedures in patients undergoing craniotomy for the resection of brain tumors and/or tissue with radiation damage. We demonstrate in three case studies the ability of this instrument to resolve distinct tissue types and pathology including cortex, white matter, tumor, and radiation-induced necrosis. In particular, two patients with effects of radiation induced necrosis exhibited longer fluorescence lifetimes and increased optical redox ratio on the necrotic tissue with respect to non-affected cortex, and an oligodendroglioma resected from a third patient reported shorter fluorescence lifetime and a decrease in optical redox ratio than the surrounding white matter. These results encourage the use of FLIm as a label-free and non-invasive intraoperative tool for neurosurgical guidance.

GRAPHICAL ABSTRACT
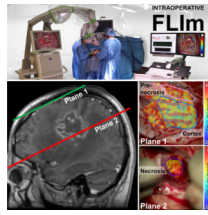
An intraoperative fluorescence lifetime imaging (FLIm) instrument is safely used during human brain surgery to resolve distinct tissue types and pathologies, as reported in three case studies. Autofluorescence lifetime contrast provides label-free biochemical information of distinct brain tissues including cortex, tumors, and radiation induced necrosis. The FLIm instrument integrates with surgical microscopes to provide real-time intraoperative augmentation of the surgical field of view with fluorescent-derived parameters encoding diagnostic information.

Keywords

1 | INTRODUCTION

Currently, surgical resection of brain tumors is primarily guided by pre-operative magnetic resonance imaging (MRI) and computed tomography (CT) imaging. These techniques play an important role in surgical planning as they help determine the best location to make an incision, the optimal path to the targeted anatomical area, and what critical structures to avoid. Such an approach, however, requires intraoperative mapping of the pre-operative images onto the surgical field[1–3]. Neurosurgeons lack intraoperative or real-time feedback, and ultimately rely on subjective evaluation of brain tissues (visual inspection or texture assessment) to distinguish between clinically relevant conditions (e.g. solid brain tumor and infiltrative edge, radiation-induced necrosis and normal brain), which can lead to a suboptimal outcome of the surgical therapy.

While advances in intraoperative MRI (iMRI) and intraoperative ultrasound (iUS) techniques have demonstrated improved surgical outcomes[3], these techniques are seldom used due to practical drawbacks. The iMRI systems require specialized operating rooms and surgical instruments that are very expensive and unavailable to many medical centers as well as time consuming. While iUS systems are affordable and can provide real-time feedback, the quality of the images is rather poor and subject to interpretation due to low resolution and moving artifacts[3].

Intraoperative optical imaging using fluorescent contrast agents has also showed promise[4]. The most prominent approach is the use of metabolic biomarkers such as 5-aminolevulinic acid (5-ALA) and protoporphyrin IX (PpIX), which is routinely used especially for guidance of glioblastoma multiforme (GBM) surgery in human patients[5–8]. More recently, EGFR-targeted molecular probe cetuximab-IRDye800[9] has also demonstrated potential to highlight highgrade gliomas during neurosurgical procedures. Despite their success in detecting high grade glioma's areas with more confined appearance, the performance of

these probes dramatically decreases at the infiltrating edge of the tumor and for low grade gliomas[5,8]. Moreover, these techniques rely on time-coordinated delivery of exogenous molecular probes to patient that have limitations in terms of both tumor specificity and uptake due to blood-brain-barrier, and clinical practicality, for example, OR lights should be dimmed to observe contrast[5].

More recently, label-free optical techniques, specifically Raman[10] and fluorescence spectroscopy and imaging[11], have emerged as a means for intraoperative guidance of neurosurgical procedures. In contrast to conventional imaging techniques noted above, the spectroscopic signatures derived from Raman and fluorescence measurements provide information about a plethora of intrinsic molecular and metabolic fingerprints in tissues and cells that might vary with tumor phenotype, heterogeneity of both normal and diseased tissue, or tissue and cellular response to therapy (e.g. radiation therapy). Recent studies employing Raman spectroscopy demonstrated the ability of this technique to differentiate normal brain invaded by high grade gliomas (tumor margins) as well as low grade gliomas using a handheld contact probe allowing for local characterization of brain tissue in vivo[10]. The autofluorecence properties of brain tissue (healthy and diseased states) measured in patients using both steady-state[12] and lifetime techniques[13] have also demonstrated the potential of resolving brain tumors from surrounding normal tissue. Earlier, our group developed a clinically compatible time-resolved fluorescence spectroscopy apparatus that has shown potential to distinguish the low- and high-grade glioma tissue from normal cortex and normal white matter based on specific spectral and temporal fluorescence characteristics[14,15]. Moreover, these studies indicated that while low-grade gliomas can be delineated with high sensitivity and specificity, the fluorescence characteristics of high-grade gliomas have a large variability, which appeared to be correlated with the heterogeneous composition of these tumors[15]. Multiphoton fluorescence lifetime imaging approaches have also been documented for intraoperative human brain tumor identification[16], which provide cellular resolution within a limited field of view.

Despite numerous advantages, these label-free techniques have been mainly implemented in a point-spectroscopy configuration where only a few 'points' (typically 2–3 small areas) are interrogated during the surgical procedure, leaving most of the surgical field of view unmapped. Here we report the integration of a scanning point-spectroscopy fluorescence lifetime system with the conventional surgical microscope used during neurosurgical procedures. The technique allows for the formation of fluorescence lifetime imaging (FLIm) maps and real-time intraoperative augmentation of the surgical field of view with fluorescence-derived parameters encoding diagnostic information. The ability of this approach to resolve in real-time distinct tissue types in the brain (e.g. cortex, radiation necrosis, tumor) was demonstrated in 3 patients (case studies).

2 | METHODS

2.1 | Study design

A FLIm prototype system was integrated with a conventional surgical microscope to evaluate FLIm as a means for label-free real-time intraoperative guidance of neurosurgical procedures. Specifically, the goal was to demonstrate whether FLIm can be used during

craniotomy procedures to evaluate tissue biochemical and functional properties within large surgical areas (ad-hoc selected by the neurosurgeon), to display and augment the optical parameters encoding diagnostic information onto neurosurgeon's field of view as seen through the surgical microscope without interfering with standard surgical practice, and to evaluate the ability of FLIm parameters to provide optical contrast that allows for distinction of clinically relevant brain conditions.

2.2 | FLIm instrumentation

The main FLIm instrumentation used in this study was reported previously[17,18]. Briefly, light from a 355 nm pulsed Nd:YAG microchip laser (pulse duration <0.6 ns, pulse energy >2 μJ, repetition rate 2 kHz, STV-02E-1×0, TEEM photonics, France) was delivered to the tissue at 120 Hz via a fiber optic probe. For the current application, we built a custom hand-held 3 m long probe consisting of a single 365 μm core multimode fiber with a strong abrasion resistant tefzel buffer (FG365UEC, Thorlabs, NJ). The probe allowed for sterilization using a readily available low-temperature, hydrogen peroxide gas plasma system. Fluorescence light generated by the tissue was collected by the same fiber and coupled into a wavelength selection module (WSM) described in detail in Yankelevich et al. [18]. The fluorescence emission is spectrally resolved in four bands or channels: 390/40 nm (Ch1, Semrock FF01–390/40–25), 470/28 nm (Ch2, Semrock FF01–470/28–25), 542/50 nm (Ch3, Semrock FF01–542/50–25), and 629/53 nm (Ch4, Semrock FF01–629/53–25). These spectral bands were tailored to the emission of matrix proteins, NADH, FAD and porphyrins, respectively extensively documented in the literature[19,20]. The optical signal from each band was temporally multiplexed using increasing length of delay fibers such that a single microchannel plate photomultiplier tube (R3809U-50, Hamamatsu, Japan) was used to detect data from the four channels sequentially. The signal from the PMT was amplified (AM-1607–3000, Miteq Inc., USA) and sampled using a 12.5 GS/s digitizer (PXIe-5185, National Instruments, TX). Light from a 445 nm continuous-wave solid-state laser (TECBL-50G-440-USB, World Star Tech, Canada) integrated in the WSM was delivered to the measured area via the same fiber optic probe. The spot from this visible beam highlighted the area of the operating field where FLIm measurements were being performed such that the measurement locations could be identified in the surgical microscope video stream. All components required for FLIm signal generation, acquisition, processing, and display were integrated into a custom movable cart (Fig. 1).

In addition, precise tracking of the measurement location enabled monitoring of tissue exposure to light to ensure compliance with the American Standard for Safe Use of Lasers ANSI Z136.1[21]. The maximum permissible exposure (MPE) can be computed by taking into account the known excitation light pulse characteristics, for example for one 355 nm pulse the MPE is equal to 0.00283 J/cm^2. The current FLIm system delivered 1.2 μJ pulses and was therefore compliant for single pulse MPE. The multiple pulse exposure is dependent on the duration of exposure in each location and is ultimately determined by the surgeon. To ensure a safe use of the system, both UV laser repetition rate (120 Hz) as well as the aiming beam power (0.25 mW) were selected to obtain a safe dwell time of 5 seconds. This value corresponds to the duration a single location can be safety exposed with the fiber in contact with tissue (see Supplemental Information for more details on MPE calculations). The

exposed locations provided by the image augmentation algorithm can be used to derive an MPE tracking function based on cumulative exposure for each pixel of the field of view. Because the actual dimension of the illumination spot is not known, the MPE tracking works under the assumption that each exposed location receives the maximum fluence allowed by the system (fiber in contact with tissue, beam diameter 400 μm). When a threshold of the maximum permissible exposure is achieved (typically 50%), the associated visualization software (see below) highlights in black the location that reached that threshold to indicate the surgeon that the area should not be further exposed. In reality, the fluence decreases with increasing fiber to tissue distance so the estimated exposure is overestimated and increases the 50% safety margin further.

2.3 | FLIm data processing and analysis

The extraction of FLIm derived parameters including spectral ratio and lifetime values was performed using a non-negative least-squares deconvolution with Laguerre expansion described elsewhere[22]. This method allowed for fast (online) and accurate analysis of fluorescence decay dynamics and for real-time computation of fluorescence lifetime values and other relevant decay parameters. It takes 33 ms for every data point to be acquired, processed, and displayed. Optical redox ratios were also computed dividing the intensities collected in channels 3 (FAD) and 2 (NADH) as indicated in Fig. 1 c[23].

FLIm data with signal-to-noise ratio (computed as the peak intensity over the standard deviation of the noise) over threshold (SNR > 25) were averaged for each imaged plane and tissue type. Comparisons between groups were analyzed by Students T-test, with significance considered for p < 0.001 and marked with * in Figures 2 – 4 and Table 1. Means and standard deviations of fluorescence lifetime for spectral channels 1, 2 and 3, as well as of optical redox ratios are reported in Table 1. For each case, histograms (violin plots) of the computed average fluorescence lifetime values and optical redox ratios distributions were generated for each tissue type involved and are displayed in Figures 2 – 4.

2.4 | Surgical microscope and software integration

A conventional surgical microscope (Pentero 900, Zeiss, Germany) was employed to demonstrate the concept of this study. The microscope camera was used to generate a high quality video stream of the surgical field during FLIm data acquisition. Based on this video stream, FLIm parametric maps derived from the point measurements were generated using a real-time augmented reality method developed by our group[24] and adapted to this study. Briefly, a visible light aiming beam integrated in the FLIm system discussed above was used to highlight the location of the surgical field where each FLIm measurement was performed (Fig. 1). The video of the surgical field of view, sent to the FLIm console, was processed to extract the aiming beam location as well as spot size while rejecting artifacts such as instrument glare. FLIm parameters were combined with the measurement location information to generate a real-time augmented reality view of the surgical field of view (see Supplemental Information video S1).

2.5 | Human patients procedures

The ability of the FLIm system to assess brain tissues biochemical properties and to augment the optical parameters on the neurosurgeon field of view as seen through the surgical microscope was tested on 3 patients undergoing conventional craniotomy for the resection of brain tumors and/or tissue with radiation damage. The study was approved by the University of California Davis Institutional Review Board. The FLIm instrument was brought to the operating room and was coupled to the surgical microscope. The distal end of a sterilized fiber optic probe was handed to the neurosurgeon. The brain areas of interest were identified by the neurosurgeon based on an intraoperative MRI-guided neuronavigation system and by visual inspection of the site of operation. The FLIm images were acquired by handheld scanning. The surgeon controlled the start/stop of data acquisition with a dedicated pedal, made ad-hoc decisions about the area to scan, and was blind to the meaning of FLIm data during the procedure. FLIm data were acquired from both brain cortex as well as deeper regions in the brain along the resection path. Tissue biopsies were taken from FLIm interrogated areas for histopathologic correlation. The location of the biopsy areas was decided based on standard clinical protocols. Only suspicious areas, according to standard of care, (e.g. radiation necrosis damage or tumor) were biopsied.

2.6 | Pathological assessment

Areas of the fluorescence maps representing tissue type (i.e. uninvolved cortex, high-grade glioma, and necrosis) were initially identified by surgeons (JB, FG) based on visual inspection and subsequently confirmed by radiologists (MB) and neuropathologist (ML). Histopathology analysis established the tissue type of each imaged area for which a biopsy was collected as part of the standard procedure (i.e. tumor and necrotic tissue). The surgeon's visual assessment and radiologist imaging notes were otherwise considered for non-biopsied tissues such as uninvolved cortex.

2.7 | MRI

Preoperative magnetic resonance (MR) imaging was obtained on a Signa HDx 1.5T MR imaging scanner (GE Healthcare, Milwaukee, Wisconsin). All subjects underwent conventional brain MR imaging evaluation. We used the following sequences: sagittal T1, axial DWI, T1, T2, GRE, FLAIR, and images following injection of 10 ml of ProHance (Bracco Diagnostics Inc. Monroe Township, NJ) in axial and coronal planes, and 3dFSPGR. The surgical approach, biopsies, and tumor resection were performed by using MRI-based volumetric stereotactic data. Following the surgery, volumetric sequence images (3dFSPGR) were reconstructed based on coordinates/planes used during surgery corresponding to the imaged areas.

2.8 | Histopathology

Standard histological procedures were performed at the UC Davis Department of Pathology and Laboratory Medicine. All resected tissue, including lesional tissue and adjacent cortex and white matter were stained by hematoxylin and eosin (H&E) staining using standard 5 μm sections of formalin-fixed, paraffin-embedded tissue[25]. To avoid subjectivity, all

histological evaluations were done by a pathologist in a blinded fashion (ML). The Institutional Review Board approved this study and patient consents were obtained.

3 | RESULTS

3.1 | FLIm and surgical microscope features and performance

Figure 1 depicts the FLIm system integrated in the surgical workflow that is able to generate FLIm-derived parametric maps overlaid on a white light reflectance image of the operating field of view provided by a standard surgical microscope. The software on the FLIm system was able to concurrently perform three tasks in real-time (33 ms/measurement): FLIm data acquisition, processing, and display. The beginning and the end of each acquisition was decided by the surgeon and it can last from 10 seconds up to 2 or 3 minutes.

The instrument provides three pivotal points for integration with the surgical workflow: acquisition of quantitative fluorescence measurements, light exposure safety features, and real-time feedback display.

First, the system allowed for the fluorescence signal of each point measurement (FWHM or illuminated area: 400–800 μm, variable with tissue to probe distance) to be sampled and processed in real-time in the FLIm console to extract quantitative FLIm-derived parameters such as average lifetime and intensity ratios that are indicative of tissue molecular makeup and optical redox ratios indicative of metabolic activities (Figs. 1 b and 1 c).

Second, the FLIm software incorporated a safety function, as the operating parameters were determined to ensure compliance with ANSI Z136 (2014). According to this standard, both single pulse and average exposure need to fall below the maximum permissible exposure (MPE) determined for the laser operating conditions. The single pulse MPE of 2.8 mJ/cm^2 is easily determined in the most critical condition where the fiber probe is in direct contact with the tissue, using the laser pulse parameters and the fiber probe core size configuration. The surgeon is continuously scanning the operation field of view with a hoovering probe, so it is unlikely that any location will receive more than the MPE. To further ensure safe operation of the FLIm system, the MPE tracking described above provides guidance to the surgeon about what areas are at risk of overexposure guaranteed.

Third, the designed software allowed for real-time data visualization (Supplemental Information video S1). The microscope video stream was processed to extract the location of each measurement (Fig. 1 d). FLIm parameter values and measurement locations were then combined to generate real-time augmented reality maps of the surgical field of view (Fig. 1 e). The augmented FLIm map refresh rate, determined by the processing of averaged FLIm measurement (4×) and extraction of aiming beam location, was 30 Hz. For a typical measurement (Fig 1 e), the SNR of 95% of the measurements was found above 45 dB, 38 dB, 33 dB and 18 dB for channels 1 to 4 respectively. During acquisition, both fluorescence lifetime and intensity ratio, for any of the four spectral channels, could be selected for display.

3.2 | Human case studies

Representative results from the scanning procedures and realtime augmentation of FLIm parameters encoding diagnostic information are detailed below for 3 case studies.

Case study 1 Figure 2 demonstrates results from a patient that underwent a right craniotomy resection of a necrotic lesion. Two surgical planes (see Fig. 2 a) were examined with FLIm. Plane 1 corresponding to a cortex area before resection (Figs. 2 b) and Plane 2 corresponding to the necrotic core exposed after resection (Fig. 2 c). The area imaged before resection revealed a large portion of non-affected cortex (blue region of interest) and a smaller area with characteristic discoloration (pink region of interest). The area corresponding to Plane 2 was identified as radiation necrosis by pre-operative MRI and confirmed as necrosis and reactive changes consistent with radiation treatment effects by histopathological evaluation of the acquired biopsy (Fig. 2 f). The biopsy from this plane revealed mostly necrosis (60%) with some reactive changes consistent with treatment effect (40%). The area corresponding to Plane 1 did not reveal necrotic changes in the pre-operative MRI. However, histopathology results on the biopsy sample taken from the discolored area showed 99% necrosis with reactive brain parenchyma.

The FLIm parameters (i.e. average lifetimes for Channels 1–3 and optical redox ratios) for the 3 tissue types imaged in this case are depicted in Figures 2 d–e, and summarized in Table 1. When compared to normal cortex, both pre-necrotic and the necrotic tissue areas showed an increase of lifetime in channel 2 and channel 3 consistent with NADH and FAD emission, respectively. The optical redox ratios (Fig. 2 e) of pre-necrotic (lower values) and necrotic areas (higher values) were also significantly different from that of not affected cortex.

Case study 2 Figure 3 shows results from a patient that underwent a left temporal craniotomy for microsurgical resection of an intra-axial necrotic lesion. Two planes were also imaged with FLIm (Fig. 3 a). Plane 1 corresponding to a cortex area that was measured after the necrotic mass was resected (Fig. 3 b) and Plane 2 corresponding to the necrotic core exposed during resection (Fig. 3 c), which was identified as radiation necrosis by the pre-operative MRI and confirmed by histopathology as necrosis with reactive brain consistent with treatment effect (Fig. 3 f). The biopsied area also contained an acute hemorrhage (bottom-left) possibly consequence of intraoperative work. The non-affected cortex tissue was not biopsied.

The FLIm parameters (Fig. 3 d–e, Table 1) had similar trends to Case 1. Compared to cortex, the necrotic tissue areas showed an increase of lifetime in channels 2 and 3. The optical redox ratio also increased in the necrotic tissue with respect to cortex.

Case study 3 Figure 4 summarizes results from a patient that underwent a right frontal craniotomy for resection of an anaplastic diffuse glioma with oligodendroglioma phenotype. Seven planes were imaged with FLIm, three of them are highlighted in Figure 4 a. Plane 1 corresponding to a cortex area measured before starting resection (Fig. 4 b), Plane 2 corresponding to an area with the tumor exposed while it was being resected (Fig. 4 c), and Plane 3 corresponding to the bottom of the resection cavity expected to be white matter (Fig.

4 d). The rest of the planes were also diagnosed by histopathology as anaplastic diffuse glioma. Non-affected cortex and white matter tissues were not biopsied.

The tumor area was confirmed by histopathological analysis (Fig. 4 g), and showed a decrease in lifetime when compared to the adjacent white matter tissue in all channels (Fig. 4 e–f and Table 1). Cortex exhibited the shortest lifetime in all channels. The optical redox ratio increased for white matter tissue with respect to cortex and tumor areas, but was indistinguishable between cortex and tumor, in this case. Figures 4 e–f display all tumor points measured in 5 different planes through resection pooled together. A break down of the tumor distribution lifetime and optical redox ratio in each plane is shown in figure 4 h to illustrate the consistency encountered throughout the tumor volume.

3.3 | Discussion

In this paper we report, to our knowledge, the first demonstration of a point-scanning FLIm technique integrated with a surgical microscope as a means for intraoperative label-free real-time image-guided neurosurgical procedures. The current study showed the ability of this techniques to 1) safe and fast map (33 ms/data point) the biochemical/functional properties of normal and diseased brain tissues based solely on tissue autofluorescence properties, 2) augment in real time the FLIm parameters encoding diagnostic information on the surgical field of view as seen through the conventional microscope used during neurosurgical procedures, and 3) identify distinct brain tissue types in patients (case studies) undergoing open scull surgery for removal of brain cancer and/or radiation necrosis.

We showed that the FLIm apparatus can be readily integrated with the surgical microscope routinely used during neurosurgical procedures using standard video output connections. The microscope was used as a venue for real-time visualization of FLIm enhanced brain tissue characteristics. In the current configuration, the neurosurgeon is able to control FLIm data acquisition, ad-hoc select the areas of interest for FLIm scanning, reduce or increase the scanning speed, revisit brain areas of interest, and choose to augment or not the FLIm parameters on the surgical field of view. An important feature of the FLIm instrumentation is the build-in safety function that allows for real-time computation of the maximum permissible exposure (MPE) and for signaling the surgeon to not re-visit areas where the MPE riches a pre-defined threshold value. Moreover, the data visualization software allows for display of any of the multiple FLIm-derived parameters based on the user need (e.g, parameters from any spectral channel of interest related to biochemical makeup and/or optical redox ratios related to tissue metabolic properties). For future studies, once a database of diagnostic features combining information from all spectral channels and classifiers are available, we anticipate to directly display diagnostic information.

While a few previous fluorescence lifetime techniques[13,15] have demonstrated their potential for intraoperative assessment of brain cancer, their earlier implementations had notable limitations. The first reported time-resolved fluorescence spectroscopy setup[15,26] used in clinical neurosurgery (patients with both low- and high-grade gliomas) was a point-spectroscopy technique that required about 30 seconds to acquire a single dataset. In a subsequent study employing a fiber-bundle based fluorescence lifetime imaging microscopy (FLIM) instrumentation (conducted in patients with high grade gliomas infiltrated in the

cortex), it required nearly 2 minutes to generate a FLIM image (~ 4 mm diameter field of view)[13]. Ultimately, this latter approach, that also required direct contact between probe and tissue, was found unsuitable for post-resection measurements due to either highly uneven brain surfaces or blood/fluid accumulation affecting the light delivered or collected from a given brain area. The FLIm system reported here not only overcomes the drawbacks of the earlier instrumentation by providing a means for fast reconstruction of fluorescence maps at any time during surgery irrespective of anatomic changes, but also allows for augmentation of FLIm images on the surgical field of view.

Effective delineation of non-affected brain tissue from brain tumor at the resection margins or tumors from radiation injury is paramount for improved patient surgical outcome. Here, we demonstrated in 3 case studies the ability of our FLIm instrumentation and technique to visualize and generate contrast between distinct types of brain tissue with relevance in surgical therapy decision making.

The two cases involving patients with radiation necrosis, demonstrated the potential of FLIm to identify areas with radiation injuries (Figures 2 and 3) from non-affected cortex. In both cases, the necrotic regions showed increased fluorescence lifetime values in all spectral channels as well as increased redox ratios. Importantly, even the early necrotic changes not visible in conventional MRI (Case 1) were detected by FLIm. These lifetime trends as well as the sensitivity of FLIm to early necrotic changes observed in human patients are consistent with a previous study[27] our group reported for a rat model of brain radiation necrosis. To our knowledge, the current study is the first to report FLIm-based detection/delineation of areas with radiation injuries in human brain in vivo. The third case demonstrates the ability of the FLIm system to map the brain tissue properties along the resection path (from the cortical surface, through tumor to the 'bottom' of the tumor infiltrated in white matter) and to provide real-time feedback for all resection planes along this path. Moreover, it shows the potential of FLIm to delineate areas with tumor from white matter (Figure 4). For this case of anaplastic diffuse glioma, IDH1 mutant we found lower lifetime and redox ratio values when compared to surrounding white matter.

While this study represents a successful demonstration of FLIm-augmented reality approach to real-time intraoperative guidance of surgical resection, the overall diagnostic value of the FLIm derived parameters will require further investigation. Since fluorescence signatures are sensitive to biochemical and metabolic conditions in brain tissue, it is expected that such signatures would vary with tumor phenotype and respective metabolic status. Thus, extensive studies in a large number of patients are needed to account for all possible tissue types and composition as well as metabolic conditions. Such studies will extend on earlier findings[15] that have indicated that low grade gliomas (including oligodendroglioma) have distinct fluorescence properties than glioblastoma multiforme (GBM). Also, they have the potential to resolve diagnostic challenges posed by the highly heterogeneous GBM's features. For example, IDH mutant gliomas have different metabolism pattern than IDH wild type, which in turn correlate to different survival out-comes[28,29]. While fluorescence-guided surgery with agents such as 5-ALA are increasingly adopted as standard practice in clinical settings to highlight GBM, their effectiveness decreases overtime and is limited in areas of low-density tumor cell infiltration[5,8]. In addition, lower grade gliomas are the

tumor types with more difficult intraoperative identification, and exogenous fluorescent markers have not yet been successful on that end. Distinguishing between recurrent GBM and radiation induced necrotic tissue is also of interest to neurosurgeons, as pre-operative MRIs are not always conclusive and treatment strategies for either case differ significantly. FLIm has the potential to address drawbacks of 5-ALA based intraoperative imaging by using the distinct autofluorescence lifetime characteristic of pathological tissue, for example as seen here with the long lifetime from necrotic tissue that could be used as a biomarker for radiation induced necrosis or by detecting low grade gliomas with high sensitivity and specificity as previously reported[15]. Importantly, surgical injury in itself may affect tissue fluorescence properties due to changes in tissue oxygenation or inflammatory response during the procedure[30]. For instance, we observed that FLIm measurements performed on cortical surface (in the proximity of excision) have slightly different fluorescence properties before and after resection. Systematic studies identifying autofluorescence changes upon tissue manipulation are needed.

Other constrain of this fiber-based FLIm method for intraoperative use is that recording of high quality (SNR) data requires a clean surgical field for UV light not be absorbed by blood. The local point scanning approach facilitates to clean up the surgical area from blood and other fluids as the image is acquired, while is more challenging to achieve in large areas for wide-filed imaging. The point scanning approach is also convenient to interrogate areas of difficult access or quickly highlight sparse areas in the field of view, but does require longer time than a wide-field image snapshot. This technique does not provide cellular resolution, hence cancerous individual cells surrounded by healthy tissue would be difficult if not impossible to detect. However, the sub-millimetre resolution provided by a 400 μm core fiber should be sufficient for the practical scale of surgical interventions.

Regardless of these limitations, the current study demonstrates the feasibility of fluorescence lifetime imaging to operate in challenging surgical environments including dynamic changes of anatomic landmarks during resection and to resolve clinically relevant brain tissue types.

4 | CONCLUSIONS

The present study demonstrates the feasibility of a scanning fluorescence lifetime imaging technique for safe and real-time intraoperative assessment of brain tissue types based solely on tissue autofluorescence properties. We showed that the FLIm technique reported here can be straightforward integrated within the surgical workflow and allows for real-time augmentation of optical parameters encoding diagnostic information on the brain surface, which can be seen by the neurosurgeon during surgery. Current results from patients undergoing neurosurgical procedures show the potential of FLIm-derived parameters to resolve, as validated by histopathology, distinct brain tissue types that are clinically relevant. These include brain tumors as well as necrotic changes in the brain in response to radiation injury. The current study provides the first evidence of the ability of FLIm to detect both early (typically not seen in MRI) and late necrotic changes.

Supplementary Material

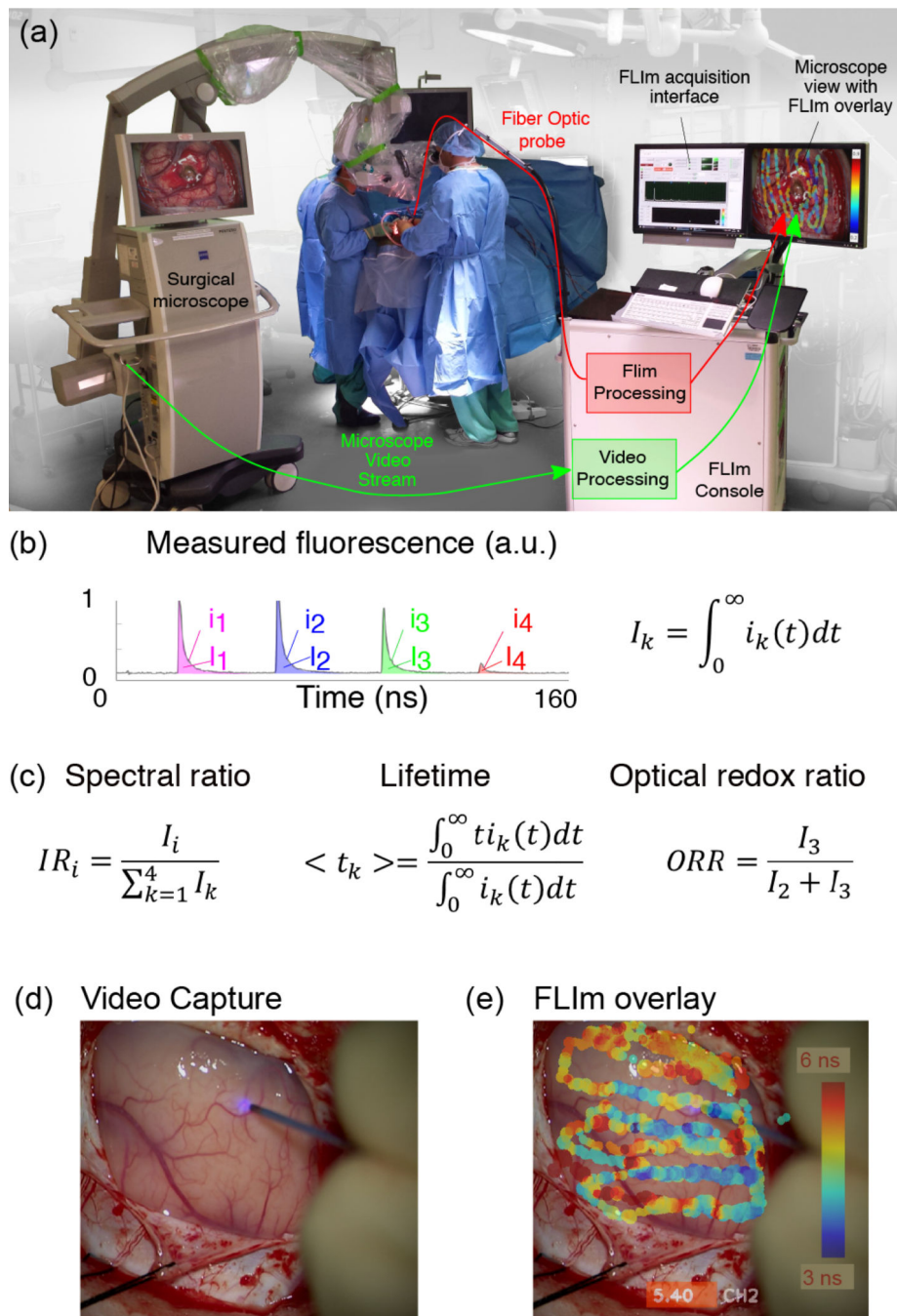Refer to Web version on PubMed Central for supplementary material.

References

[1]. Jenkinson MD, Barone DG, Bryant A, Vale L, Bulbeck H, Lawrie TA, Hart MG, Watts C, Cochrane Database of Systematic Reviews 2018 (1).

[2]. Miner Robert C., Journal of Medical Imaging and Radiation Sciences 2017,48 (4), 328–335. [PubMed: 31047466]

[3]. Hu Shuang, Kang Homan, Baek Yoonji, Fakhri Georges El, Kuang Anren,Choi Hak Soo, Advanced Healthcare Materials 2018, 7 (16), 1–15.

[4]. Pogue Brian W, Gibbs-Strauss Summer, Valdés Pablo A, Samkoe Kimberley, Roberts David W, Paulsen Keith D, IEEE journal of selected topics in quantum electronics: a publication of the IEEE Lasers and Electro-optics Society 2010,16 (3), 493–505.

[5]. Stepp Herbert, Stummer Walter, Lasers in Surgery and Medicine 2018, 50, 399–419. [PubMed: 29737540]

[6]. Lara-Velazquez Montserrat, Al-Kharboosh Rawan, Jeanneret Stephanie, Vazquez-Ramos Carla, Mahato Deependra, Tavanaiepour Daryoush, Rahmathulla Gazanfar, Quinones-Hinojosa Alfredo, Brain Sciences 2017, 7 (166), 16.

[7]. Valle Ricardo Díez, Hadjipanayis Constantinos G., Stummer Walter, Journal of Neuro-Oncology 2019,141 (3), 487–494. [PubMed: 30607705]

[8]. Hadjipanayis Costas G, Widhalm Georg, Stummer Walter, Neurosurgery 2016, 77 (5), 663–673.

[9]. Miller Sarah E., Tummers Willemieke S., Teraphongphom Nutte, van den Berg Nynke S., Hasan Alifia, Ertsey Robert D., Nagpal Seema, Recht Lawrence D., Plowey Edward D., Vogel Hannes, Harsh Griffith R., Grant Gerald A., Li Gordon H., Rosenthal Eben L., Journal of Neuro-Oncology 2018,139 (1), 135–143. [PubMed: 29623552]

[10]. Desroches Joannie, Lemoine Émile, Pinto Michael, Marple Eric, Urmey Kirk, Diaz Roberto, Marie Christine Guiot Brian C. Wilson, Petrecca Kevin, Leblond Frédéric, Journal of Biophotonics 2019 (October 2018), 1–7.

[11]. Marcu Laura, Hartl Brad A., IEEE Journal on Selected Topics in Quantum Electronics 2012,18 (4), 1465–1477. [PubMed: 28053498]

[12]. Toms Steven A., Lin Wei Chiang, Weil Robert J., Johnson Mahlon D., Jansen E. Duco, Mahadevan-Jansen Anita, Neurosurgery 2005, 57 (4 SUPPL), 382–391. [PubMed: 16234690]

[13]. Sun Yinghua, Journal of Biomedical Optics 2010,15 (5), 056022.

[14]. Yong William H., Butte Pramod V., Pikul Brian K., Jo Javier A., Fang Qiyin, Papaioannou Thanassis, Black Keith L., Marcu Laura, Frontiers in Bioscience 2006, 11, 1255. [PubMed: 16368511]

[15]. Butte Pramod V, Mamelak Adam N., Nuno Miriam, Bannykh Serguei I., Black Keith L, Marcu Laura, Neuroimage 2011, 54 (1), S125–S135. [PubMed: 21055475]

[16]. Kantelhardt Sven R., Kalasauskas Darius, Karsten König, Kim Ella, Weinigel Martin, Uchugonova Aisada, Giese Alf, Journal of Neuro-Oncology 2016, 127 (3), 473–482. [PubMed: 26830089]

[17]. Ma Dinglong, Bec Julien, Gorpas Dimitris, Yankelevich Diego, Marcu Laura, Biomedical Optics Express 2015, 6 (3), 987. [PubMed: 25798320]

[18]. Yankelevich Diego R., Ma Dinglong, Liu Jing, Sun Yang, Sun Yinghua, Bec Julien, Elson Daniel S., Marcu Laura, Review of Scientific Instruments 2014, 85, 034303.

[19]. Berezin Mikhail Y, Achilefu Samuel, Chemical Reviews 2011,110 (5), 2641–2684.

[20]. Marcu Laura, French Paul MW, Elson Daniel S, Fluorescence lifetime spectroscopy and imaging: principles and applications in biomedical diagnostics, CRC Press, 2014.

[21]. ANSI Z136.1 Safe use of Lasers, 2014.

[22]. Liu Jing, Sun Yang, Qi Jinyi, Marcu Laura, Physics in Medicine and Biology 2012, 57 (4), 843–865. [PubMed: 22290334]

[23]. Skala Melissa C, Riching Kristin M, Gendron-fitzpatrick Annette, Eickhoff Jens, Eliceiri Kevin W, White John G, Ramanujam Nirmala, PNAS 2007, 104 (49), 19494–19499.

[24]. Gorpas Dimitris, Ma Dinglong, Bec Julien, Yankelevich Diego R., Marcu Laura, IEEE Trans Med Imaging 2016, 35 (8), 1802–1811. [PubMed: 26890641]

[25]. Slaoui Mohamed, Laurence Fiette in Drug Safety Evaluation: Methods and Protocols, Methods in Molecular Biology, Vol. 691, Springer Science+Business Media, LLC, 2011, chapter 4, pp. 69–82.

[26]. Butte Pramod V, Fang Qiyin, Jo Javier A, Yong William H, Pikul Brian K, Black Keith L, Marcu Laura, Journal of biomedical optics 2010,15 (2), 27008.

[27]. Hartl Brad A., Ma Htet S.W., Sridharan Shamira, Hansen Katherine S., Kent Michael S., Gorin Fredric, Fragoso Ruben C., Marcu Laura, Biomedical Optics Express 2018, 9 (8), 3559. [PubMed: 30338140]

[28]. Strickland Marie, Stoll Elizabeth A., Frontiers in Cell and Developmental Biology 2017, 5 (April).

[29]. Quinones Addison, Le Anne, The Multifaceted Metabolism of Glioblastoma, Le Anne(Ed.), Springer International Publishing, Cham, 2018, pp. 59–72.

[30]. Lagarto João L., Phipps Jennifer E., Faller Leta, Ma Dinglong, Unger Jakob, Bec Julien, Griffey Stephen, Sorger Jonathan, Farwell D. Gregory, Marcu Laura, Journal of Photochemistry and Photobiology B: Biology 2018,185 (April), 90–99.

(b) Measured fluorescence (a.u.)

$$I_k = \int_0^\infty i_k(t)dt$$

(c) Spectral ratio

$$IR_i = \frac{I_i}{\sum_{k=1}^4 I_k}$$

Lifetime

$$< t_k > = \frac{\int_0^\infty t\, i_k(t)dt}{\int_0^\infty i_k(t)dt}$$

Optical redox ratio

$$ORR = \frac{I_3}{I_2 + I_3}$$

(d) Video Capture

(e) FLIm overlay

FIGURE 1.

Integration of the FLIm system in the neurosurgical operating room. (a) FLIM in the operating room and integration in the surgical workflow. The surgeon scans the surgical field with a hand-held fiber optic probe that allows for delivery of excitation, collection of tissue autofluorescence, and delivery of the aiming beam; (b) Example of a data set acquired from point measurement ('Pixel') depicting the fluorescence decays on the FLIm4 spectral channels; (c) Formulas used for online spectral ratios and average lifetime computation, (d)

White light image as typically seen through the surgical microscope; (e) White light image with augmented white light image.
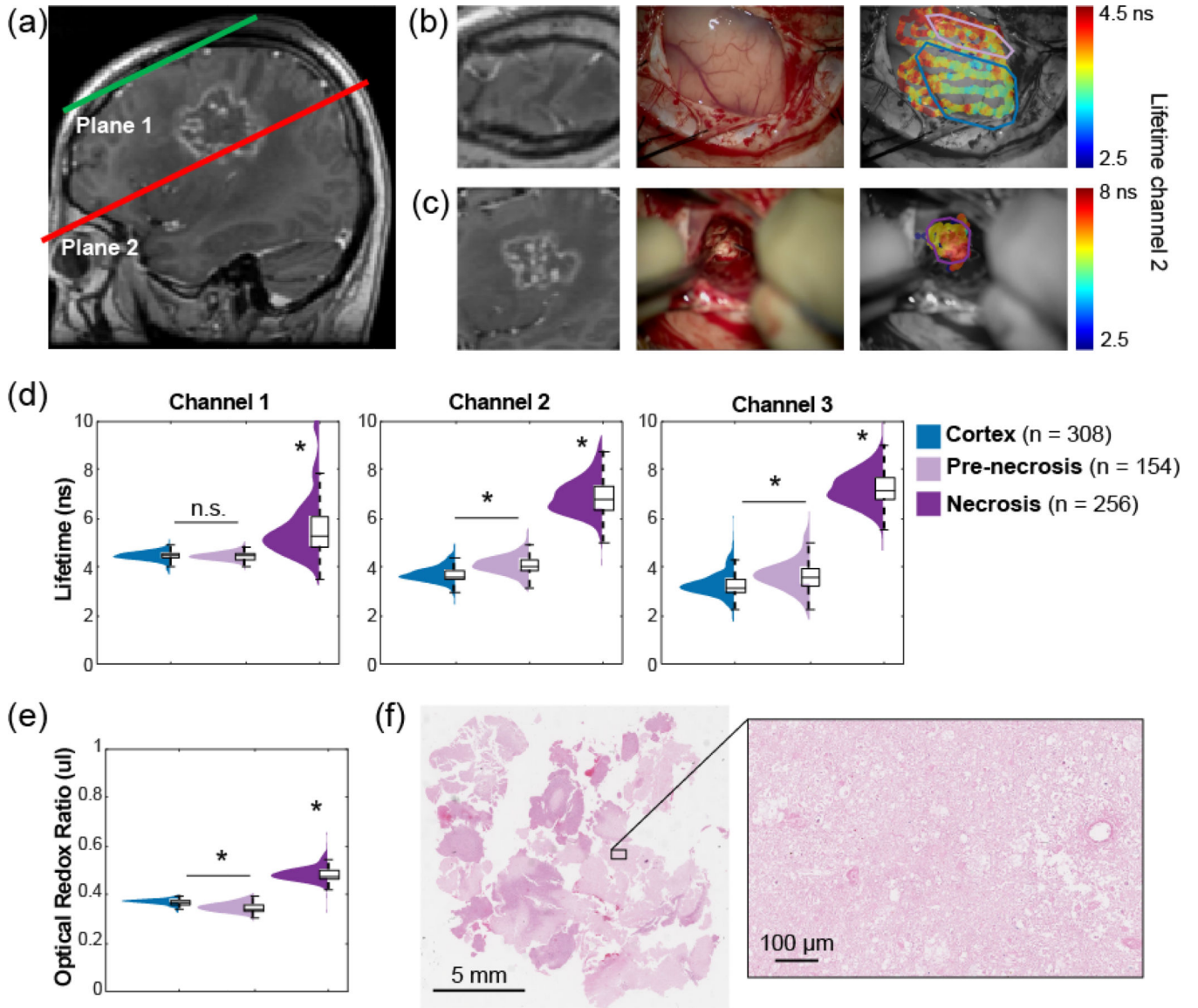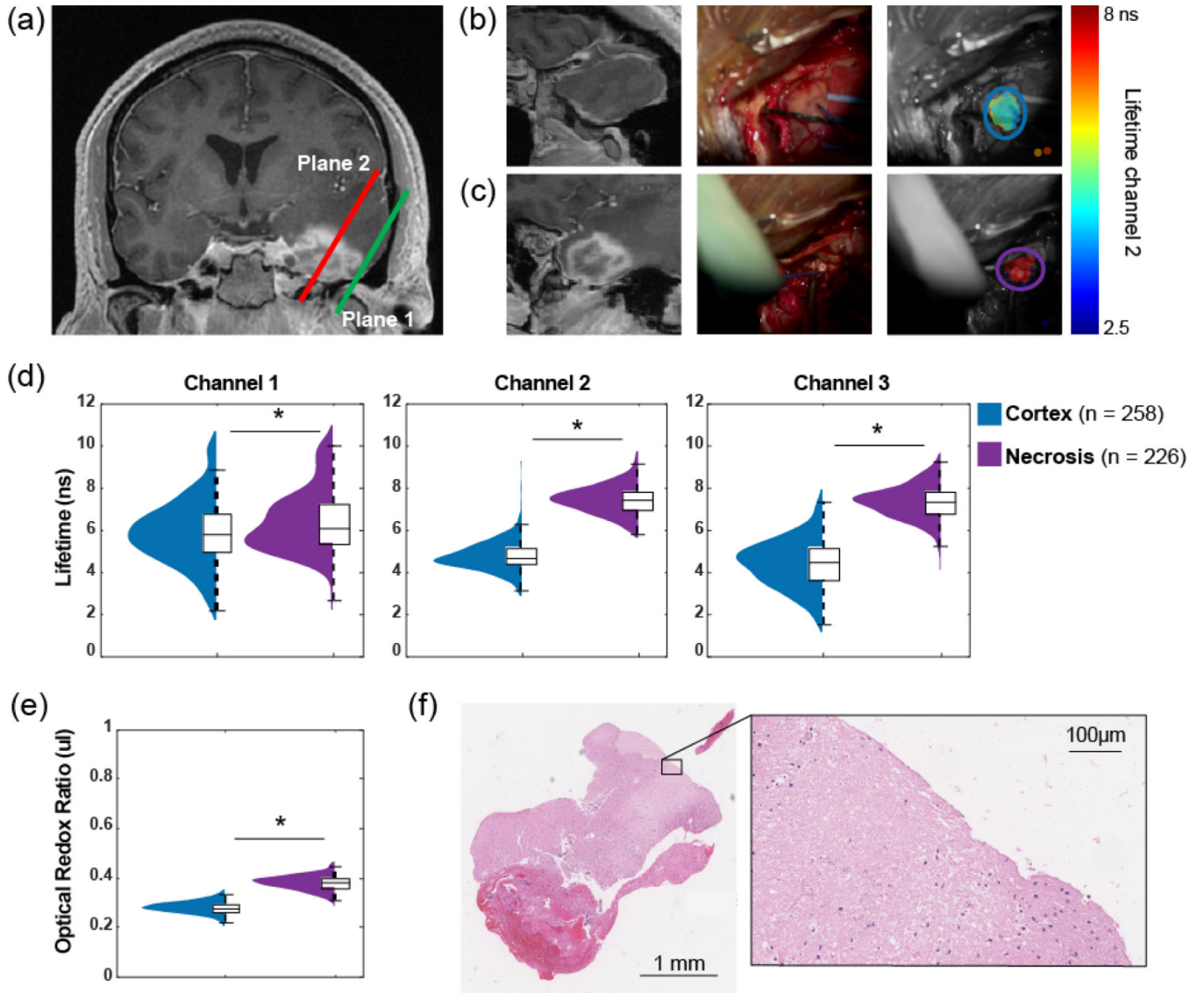
FIGURE 2.

Case study 1 from a patient with history of brain metastasis and radiation therapy. a) MRI sagittal view of patient's brain. Details of b) Plane 1 before resection, and c) Plane 2 with the necrotic core exposed (MRI of imaged planes, left panel; surgical field of view, middle panel; surgical field of view with augmented FLIm map (Channel 2) and delineated tissue areas, right panel). d) Average lifetime values distributions, and e) optical redox ratio for each highlighted tissue area (in right panels b, c), for channels 1, 2, and 3. *n* indicates the number of measurement points. * p < 0.001, n.s. non-significant, Student's T-test. f) H&E stains of biopsied necrotic area in Plane 2.

FIGURE 3.

Case study 2 from a patient with history of nasopharyngeal carcinoma for which the patient had received radiation therapy, and presented with a left temporal ringenhancing lesion suspicious of radiation necrosis. a) MRI sagittal view of patient's brain. Details of b) Plane 1 exhibits a cortical area, and c) Plane 2 has the necrotic core exposed (MRI of imaged planes, left panel; surgical field of view, middle panel; surgical field of view with augmented FLIm map (Channel 2) and delineated tissue areas, right panel). d) Average lifetime value distributions, and e) optical redox ratio for each highlighted tissue area (in right panels b, c), for channels 1, 2, and 3. *n* indicates the number of measurement points. * p < 0.001, n.s. non-significant, Student's T-test. f) H&E stains of biopsied necrotic area in Plane 2.
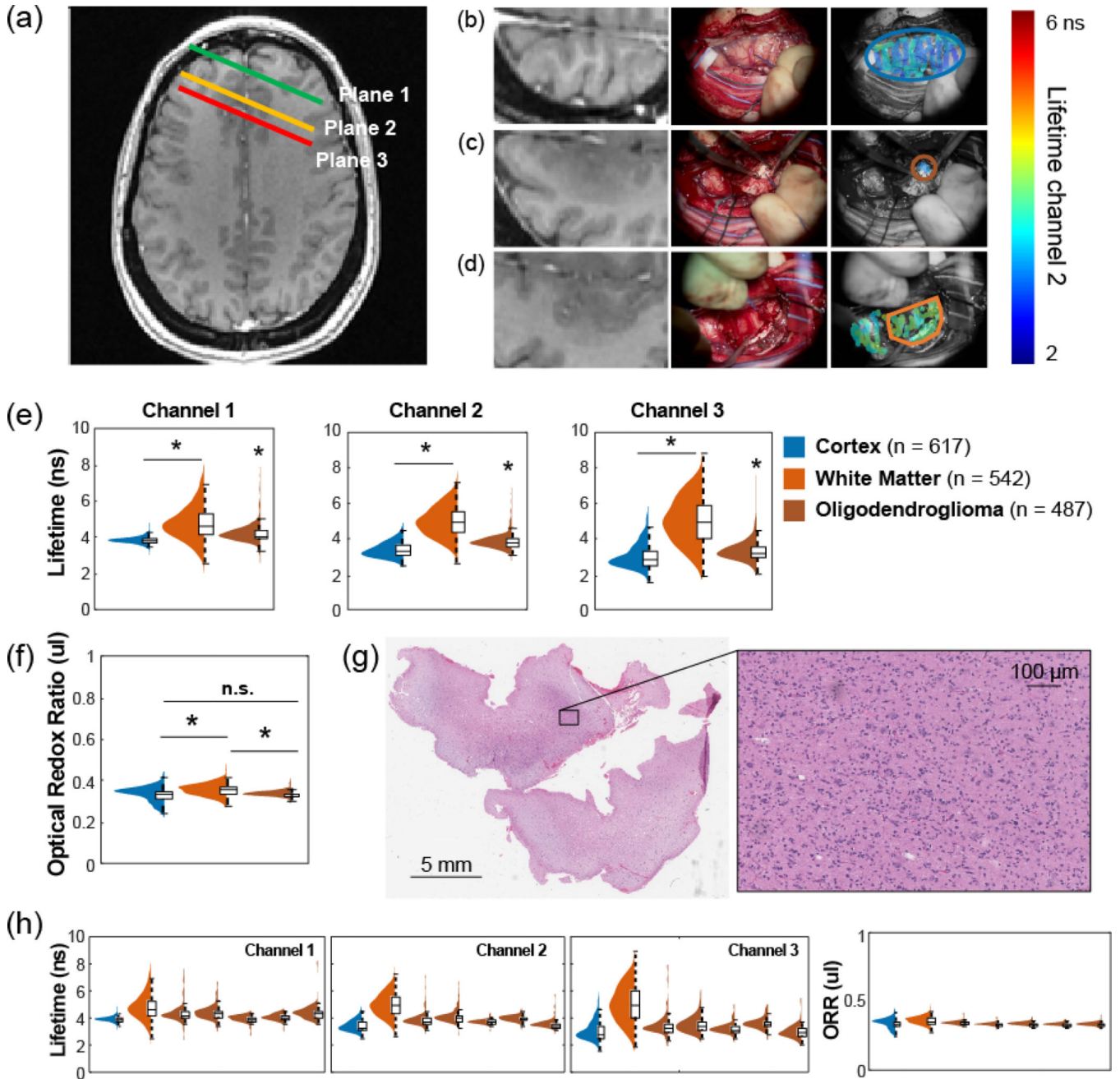
FIGURE 4.
Case study 3 from a patient with anaplastic diffuse glioma, W.H.O. grade 3 (oligodendroglioma phenotype) IDH 1c.394>T (p.R132C) mutant, 1p19q no-codeleted. a) MRI axial view of patient's brain. Details of b) Plane 1 before resection, c) Plane 2 during resection, and d) Plane 3 at the bottom of the surgical resection cavity (MRI on the imaged plane, left panel; surgical field of view, middle panel; surgical field with augmented FLIm map (Channel 2) and delineated tissue areas, right panel). e) Fluorescence lifetime distributions, and f) optical redox ratio for each highlighted tissue area (in right panels b, c, d) for channels 1, 2, and 3. n indicates the number of measurement points. * $p < 0.001$, n.s.

non-significant, Student's T-test. g) H&E stains of a biopsied area in the tumor plane. h) Detailed fluorescence lifetime distributions and optical redox ratio (ORR) including 5 separate tumor planes imaged during resection.

TABLE 1

Average and standard deviation of fluorescence parameters (average lifetime) for channels 1,2, and 3, and optical redox ratio for tissue types cortex, white matter, tumor, and necrosis as pertinent for each case study. Last columns indicate the level of significance when comparing tissue types (Case 1: A = cortex vs pre-necrosis, B = cortex vs necrosis. Case 2: A = cortex vs necrosis. Case 3: cortex vs tumor, B = white matter vs tumor), as determined by Student's T-test with p < 0.001 (*) and p > 0.001 (non-significant).

Case 1		Cortex	Pre-necrois	Necrosis	A	B
	Ch1	4.5 ± 0.2	4.4 ± 0.2	6 ± 1	0.3	*
Lifetime (ns)	Ch2	3.7 ± 0.3	4.1 ± 0.4	6.9 ± 0.8	*	*
	Ch3	3.2 ± 0.5	3.7 ± 0.7	7.2 ± 0.7	*	*
Optical redox ratio (ul)		0.37 ± 0.01	0.34 ± 0.02	0.48 ± 0.03	*	*

Case 2		Cortex	Necrosis		A	
	Ch1	6 ± 1	7 ± 1		*	
Lifetime (ns)	Ch2	4.7 ± 0.7	7.6 ± 0.6		*	
	Ch3	4 ± 1	7.6 ± 0.7		*	
Optical redox ratio (ul)		0.28 ± 0.02	0.38 ± 0.03		*	

Case 3		Cortex	White matter	Tumor	A	B
	Ch1	3.8 ± 0.2	4.8 ± 0.9	4.2 ± 0.5	*	*
Lifetime (ns)	Ch2	3.4 ± 0.4	4.9 ± 0.8	3.8 ± 0.5	*	*
	Ch3	2.9 ± 0.7	5 ± 1	3.3 ± 0.6	*	*
Optical redox ratio (ul)		0.33 ± 0.03	0.35 ± 0.03	0.33 ± 0.01	0.2	*